PHASE-AVERAGED MIXING CHARACTERISTICS OF MULTI-JETS MODIFIED BY CYCLIC PERTURBATION

E. Shinohara[*], *K. Tatsumi, M. Mizuno and K. Nakabe*

Graduate School of Engineering, Kyoto University, Kyoto 606-8501, Japan
* Toyota Industries Corporations, Kariya, Aichi 448-8671, Japan

ABSTRACT

Effects of a jet perturbation on mixing performance of an air-jet array were investigated experimentally. The jet array consists of three same-sized parallel jets, and the mass flow rate of the central jet is perturbed in a pulsatile or sinusoidal cycle with the frequency, f_r = 0, 1 or 2Hz. The jet array discharged simultaneously without the jet perturbation (f_r = 0Hz) shows good mixing performance in comparison with the jet array of three arithmetically-superimposed single jets. The flow condition with the jet perturbation (f_r = 1 or 2Hz), on the other hand, is alternately changed, laminar or turbulent, in one cycle of the central jet perturbation. The time-averaged velocity profiles of the jet array obtained under certain perturbed conditions demonstrate an adverse change of the mixing performance at the locations near the nozzle and far downstream. Phase-averaged velocity profiles were thoroughly examined in order to understand such a mixing mechanism of the multiple jet flow.

INTRODUCTION

Mixing of fluids is a key technology of thermo-fluid engineering, for example, to control chemical reaction processes in industrial plants, to enhance heat transfer from target surfaces of energy devices and to reduce air pollution of exhaust emissions from burners of boiler and furnaces. In chemical reactors, heat transfer units or combustors, turbulent jets are typically used to enhance the mixing of chemical agents, fuels, oxidizers, etc. The detail characteristics of the jet flows in turbulent Reynolds number regimes have been considerably investigated and known well in engineering literature. Recently, the sizes of channels and nozzles in the reactors and combustors are required to become small, which is combined with gradually popularizing distributed energy systems, e.g. micro gas turbines (MGT) or fuel cell (FC), and also developing an ultra-fine processing technology, i.e. micro total analysis systems (μ-TAS) and power micro electro-mechanical systems (power-MEMS). In the cases of such millimeter- or sub-millimeter-scale hardware, the representative jet Reynolds number becomes small because of the limitations of jet nozzle size and jet flow rate. Thus, the jet flows are situated in the laminar flow regime, and the mixing performance of the jets is restrained excessively in comparison with turbulent jet mixing.

In order to control the mixing of laminar jets, the authors have been focusing on the interaction of laminar jets and also on the jet perturbation with a pulsatile or sinusoidal cycle. We previously investigated on the mixing characteristics of a triple laminar jet array and quantitatively showed that the jet array discharged simultaneously attained better mixing than the jet array of three arithmetically-superimposed single laminar jets [1].

It was also found that, in certain cases of the central jet perturbation, a good mixing was found in the near-field of the jet nozzle while a poor mixing was in far-field, compared to the case without the perturbation. In order to elucidate this mixing tendency of the jet array perturbed by the pulsatile jet, detail investigation on the mixing characteristics of the jet array is performed experimentally in the present study.

EXPERIMETAL SET-UP

Experimental Apparatus
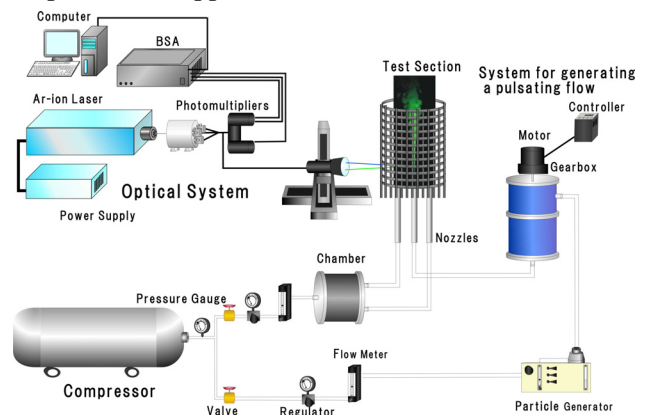
Fig. 1   Experimental apparatus.

Figure 1 shows the experimental apparatus of the triple jets issuing into the stationary atmosphere with a room temperature. The atmosphere was an open, wide and calm space which was surrounded by 100-mesh wire gauze (0.1mm in diameter) to suppress disturbances from outside. Air, as the working fluid, was supplied from a compressor to three jet nozzles. The nozzles were situated in parallel with the same inner diameter of d = 4mm, constituting a triple jet array. The jet flow from the nozzle located in the center of the array was generated pulsatingly by a mechanically-rotating valve system. This system was composed of a cylindrical chamber and two identical round disks piled inside the chamber. Two holes, 20mm in diameter, were drilled symmetrically with respect to the center in each disk. One disk was rotated by a DC electric motor while the other was held in the chamber. Thus, the flow rate was periodically changed with the pop-out discharge, depending on the disk rotation. Time-averaged volume flow rate of the jet supplied to each nozzle was monitored with a flow meter, and the maximum flow rate was obtained when the hole locations of the two disks match with each other. This system was alternatively replaced with the other device, which was invented by Durst et al. [2], in order to feed the jet fluid with a precise sinusoidal change of the flow rate.

For both the flow visualization with a high resolution CCD camera and the velocity measurement with a two-dimensional laser Doppler anemometry (LDA) system, a particle generator (TSi, model 9306) was installed at the location between the flow meter and the nozzle discharging the jet fluid as a visualizing object.

The arrangement of the jet nozzles is shown in Fig. 2. Three jet nozzles were aligned closely to each other. As is convenient for further discussion, hereafter, the center jet will be referred to as C-jet and the two other side jets as S-jets. The left-hand side jet is named more specifically as S_L-jet and the right-hand side jet as S_R-jet. The separation distance between the centers of C-jet and S_R-jet (or S_L-jet) was fixed at L = 5.9mm in the present study. The nozzle tip was sharpen and tapered by 45°.
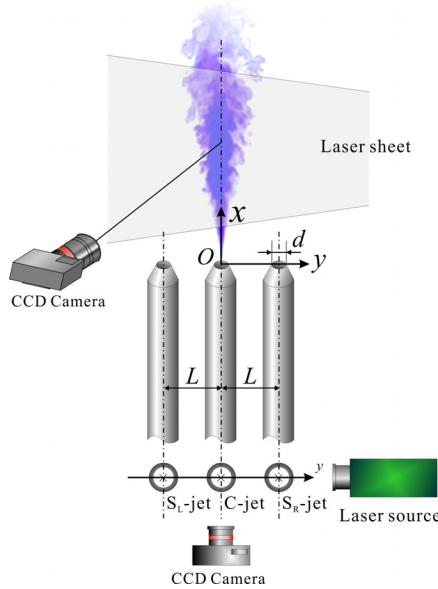
Fig. 2   Jet array arrangement.

The schematic illustration of the laser sheet to visualize the jet flows is also shown in Fig. 2. A small amount of oil mist, DEHS (Di-Ethyl-Hexyl-Sebacate), used as tracer particles, was produced by the aforementioned particle generator and was mixed into the air upstream of the jet nozzle. The nominal diameter of the oil mist particle was 1.0μm. The mist-laden jet flows were illuminated by a light sheet of an Nd:YAG pulsed laser through a cylindrical lens, and the snapshots of the flow patterns were taken using the CCD camera. The wavelength of the laser was 532nm. The picture frame of CCD camera was synchronized with the laser pulse and the maximum frame rate was 30frames per second. The spatial velocity vector maps were also obtained using PIV system when the Nd:YAG laser was emitted twice in a short series of the pulse every 1/15 seconds.

Time-dependent local velocity of the jet flow was measured using the LDA system, instead of the Nd:YAG laser and the CCD camera. In this system, two pairs of laser beams, emitted from an Argon-ion laser having the wavelengths of 488nm and 514.5nm, were guided through a laser light fiber probe (DANTEC) which was used at the location similar to that for the CCD camera. The Doppler

burst signals of the scattering light from the tracer particles back to the probe were recorded and analyzed by a signal processor (DANTEC, BSA F50), which was linked to and controlled by a personal computer.

Flow Conditions with and without Jet Perturbation

The steady jet flows without the central jet perturbation were visualized, as shown in Fig. 3. These three images in order from left-hand side correspond to the cases of single, twin and triple jets, respectively. All the flow rates of the jets were fixed at the same, the corresponding jet Reynolds number of which was Re = 1,500. The definition of the jet Reynolds number is defined as follows:

$$Re \equiv \frac{U_m d}{\nu}, \quad U_m = \frac{Q}{S} \qquad (1)$$

U_m and ν indicate a mean axial velocity of jet and a kinetic viscosity of air, respectively. U_m was calculated with a time-averaged volumetric flow rate, Q, and a cross-sectional area of the nozzle, S. Q was estimated using the velocity profile obtained experimentally in the vicinity of the nozzle exit, at x/d = 0.25, which quantitatively agrees well with the theoretical profile assumed on the basis of Hagen-Poiseuille's law. The deviation from the theoretical values was estimated within less than 1.6%.
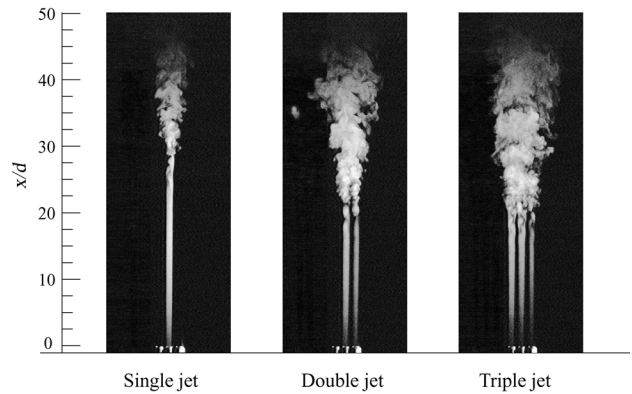
Fig. 3   Snapshots of steady jet flows (Re = 1,500).

In each snapshot of Fig. 3, the meandering area of the jet column is seen, and this area approaches the nozzle exit as the number of the jet increases. This implies qualitatively that the interaction of multiple jets enhances the fluid mixing. The time-averaged axial velocity distributions of the triple jet case of Fig. 3 are shown in Fig. 4 to quantitatively examine the mixing performance enhanced by the multiple jet interaction. The velocity profiles were measured in the spanwise direction at six different streamwise locations, i.e. x/d = 0.25, 10, 20, 25, 30 and 40, and were normalized by U_0 which is the time-averaged central streamwise velocity of C-jet measured at $(x/d, y/d) = (0.25, 0)$. The x-y spatial coordinate system is originated at the center of the C-Jet nozzle exit. The centers of S_R-jet and S_L-jet are located, respectively, at y/d = ±1.48. The solid circle (•) indicates the result obtained in the case that all three jets are simultaneously discharged. The open diamond (◊) depicts the result obtained by linearly superimposing the velocity distributions of a

single jet assuming that each jet is independent of the others.

At the locations of x/d = 0.25, 10 and 20 in Fig. 4, the velocity distributions of the two cases, • and ◊, are almost the same, pointing out that no interaction occurs among the jets near the nozzle exit. At x/d = 25, the maximum peak of each jet decreases in the case of the simultaneously-discharged triple jet, and the velocity distribution exhibits a somewhat wider pattern due to laminar jet diffusion and its interaction. At x/d = 30, a noticeable difference between the two distributions was observed, where the peak of the velocity profile in the simultaneously-discharged case conspicuously lowers and the outside flank of the distribution rises, namely, a flatter distribution was observed in this case because of the transition from laminar to turbulent of the flow. The superimposed jet case predicted a similar trend further downstream, at around x/d = 40. This comparison demonstrates that the interaction of multiple jets causes nonlinearly an early transition from laminar flow to turbulent one and a better mixing of fluids.
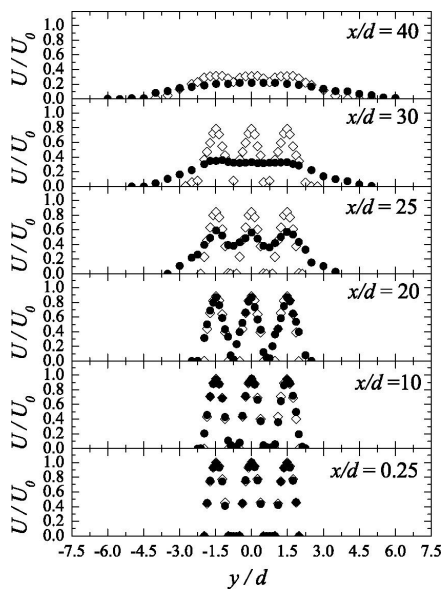
Fig. 4 Velocity profiles of steady triple jet flow (•: Simultaneous discharge, ◊: Superimposition, Re = 1,500).

Next, in order to investigate the fundamental flow characteristics of the triple jet influenced by the central jet perturbation, the MFC which can feed the jet fluid precisely in a time-dependently sinusoidal fashion was used to perturb the C-jet flow. The data obtained using MFC was referred to for the hereinafter-described results in the following section. The flow conditions of C-jet are tabulated in Table 1. The jet Reynolds number was fixed at Re = 1,500 with the constant time-averaged flow rate. The parameter, A, used in Table 1 indicates an amplitude of the sinusoidal jet velocity fluctuation. In the case of A = 0.27, the flow field showed no mixing patterns within the axial distances, $0 \leq x/d \leq 20$, independent of the perturbation frequency, fr, since the velocity of the central jet in this case changed only within the laminar flow regime. An increase of the amplitude in the cases of A =

0.63 and 078 makes the central jet a transition between laminar and turbulent flows, resulting in a better mixing performance in the near-field of the nozzle.

Table 1 Conditions of jet perturbation by MFC.

Type	Re	Frequency fr [Hz]	Amplitude A/U_0
C-jet	1.5×10^3	0	0
		1	0.27
			0.63
			0.78
		2	0.27

Following the above-mentioned examination, the mechanically-rotating valve system was used to emphasize the transition of the central jet from laminar flow to turbulent one and to expect a better mixing enhancement. The typical time-sequential flow patterns in this case are shown in Fig. 5. The disk of the mechanically-rotating valve system made a full turn with the rate of rotation, 30rpm, and then a high-speed pop-out C-jet flow was discharged twice at a regular interval in one rotation of the disk. Thus, the frequency of jet perturbation, fr, is equal to 1Hz. 10 images of Fig. 5 were taken with the time interval of 0.2s. The number assigned to each image in Fig. 5, #1 ~ #5 or #6 ~ #10, denotes the phase, $1/(5fr)$, $2/(5fr)$, ~ , $5/(5fr)$ of the first half or the second half of one disk rotation, respectively.
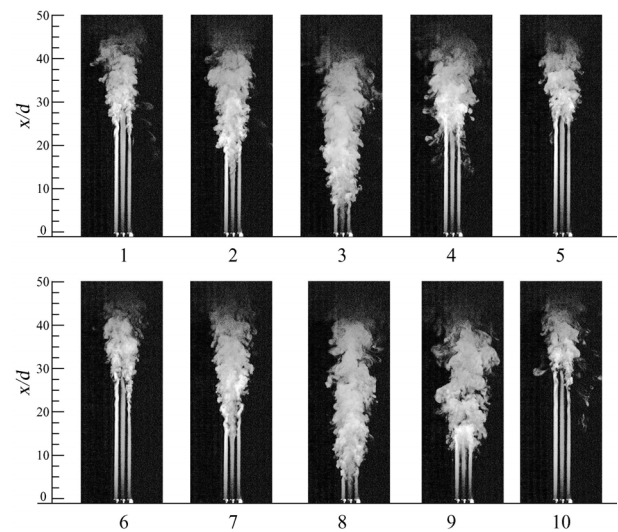
Fig. 5 Time-sequential images of the triple jet flow with perturbation in one period of the disk valve rotation (f_r = 1Hz, Re = 1,500).

Mixed-up regions of the triple jet as cloud-like shapes were clearly visualized in each image of Fig. 5, showing that the bottom edge of the mixed-up region moves up and down in response to the time-dependent flow rate of C-jet. It could be confirmed that the neighboring S-jets are significantly influenced by the pop-out C-jet perturbation. At the phases which have a maximum flow rate of C-jet with an every 1.0s interval, the three jet fluids were mixed

well together even near the nozzle exit, corresponding to the visualized images, #3 and #8.
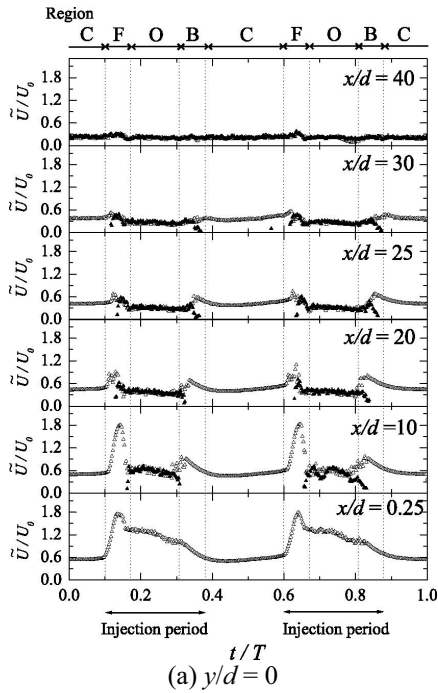
(a) $y/d = 0$
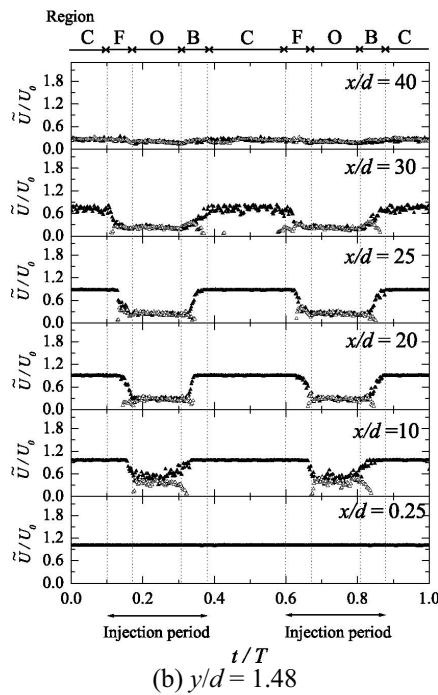
(b) $y/d = 1.48$

Fig. 6 Time histories of axial velocity with jet perturbation (Open triangle: tracer injection to C-jet, Solid triangle: tracer injection to S_R-jet, $Re = 1,500$).

Figure 6 (a) and (b) shows the time histories of streamwise velocity of the triple jet under the same flow condition of Fig. 5. The monitoring locations, (a) $y/d = 0$ and (b) $y/d = 1.48$, correspond to the centers of C-jet and S_R-jet, respectively. Four characters, C, O, F and B in each graph are assigned to the following four classified regions: the closing period of the valve, the opening period, the

forward period before full opening, and the backward period after full opening, with the rotational valve holes matching. Thus, the time period, F+O+B, is regarded as the total pop-out injection period of C-jet. An open triangle $\triangle$ plotted in Fig. 6 indicates the result measured in the case that the tracer particles were mixed in C-jet, while a solid triangle $\blacktriangle$ indicates the result with the tracer particles mixed only in S_R-jet. The ordinate of the graph is the phase-averaged streamwise velocity normalized by U_0 and defined in the following paragraph.

Concerning the data processing procedure of the jet perturbation case, an instantaneous streamwise velocity, $u(t)$, is regarded as the addition of time-averaged velocity, U, and velocity fluctuation, $U'(t)$, and also as the addition of phase-averaged velocity, $\widetilde{U}$, and another velocity fluctuation, $u'(t)$ as described in Eq. (2). Velocity data measured during $5 \sim 10$ rotations of the disk valve was used to calculate a phase-averaged velocity. The same definitions are adopted also for a instantaneous lateral velocity, $v(t)$.

$$\begin{cases} u(t) = U + U'(t) = \widetilde{U} + u'(t) \\ v(t) = V + V'(t) = \widetilde{V} + v'(t) \end{cases} \quad (2)$$

In Fig. 6 (a), no data plotted with solid triangle was observed adjacent to the nozzle exit, at the location of $x/d = 0.25$, implying that no interaction between C-jet and S-jets occurs there. At the rest of the measuring x/d locations, the contribution of S_R-jet data to C-jet is clearly recognized in O-region with a considerable coincidence of the S-jet data with the C-jet data. Besides the O-region, the latter half of F-region and the former half of B-region have also some contributions of S_R-jet because of the starting and finishing periods of the laminar-to-turbulent transition of C-jet leading to the jet interaction. In Fig. 6 (b), the contribution of C-jet data to S_R-jet was recognized, as vice versa, in the same injection period of F-, O- and B-regions.

During the period of O-region, the phase-averaged streamwise velocity becomes comparatively lower since the C-jet of O-region is already a turbulent flow and diffuses to the surroundings due to high momentum exchange. In F- and B-regions, C-jet fluid flows in transition between laminar and turbulent of the flow. The peaks observed in these two regions can be regarded as the apparent critical velocities of the flow transition.

RESULTS AND DISCUSSION

Effects of the perturbed C-jet on the neighboring S-jets are discussed in this section. Figure 7 (a) and (b) shows the time-averaged streamwise and lateral velocity distributions, U and V, of the perturbed jet case in comparison with the corresponding steady jet case under the same jet Reynolds number, $Re = 1,500$. Both velocities are normalized by U_0. The solid and open circles, $\bullet$ and $\circ$, represent the cases of the steady and perturbed jets, respectively.

In Fig. 7 (a), the perturbed jet case possesses a bit smaller velocity near the C-jet nozzle, at $x/d = 0.25$, than the steady jet case. This becomes more obvious at the streamwise locations of $x/d = 10$, 20 and 25 where the jet center velocity decreases more rapidly in the perturbed jet case compared to the steady jet case. The corresponding

lateral velocity of the perturbed jet case shown in Fig. 7 (b), in particular at $x/d = 10$, has a point-symmetric distribution with respect to the central jet axis, deducing that the central jet fluid was convected equally to the right and left sides by the jet perturbation and thus a spanwisely-wider velocity distribution was obtained.

(a) Streamwise velocity

(b) Lateral velocity
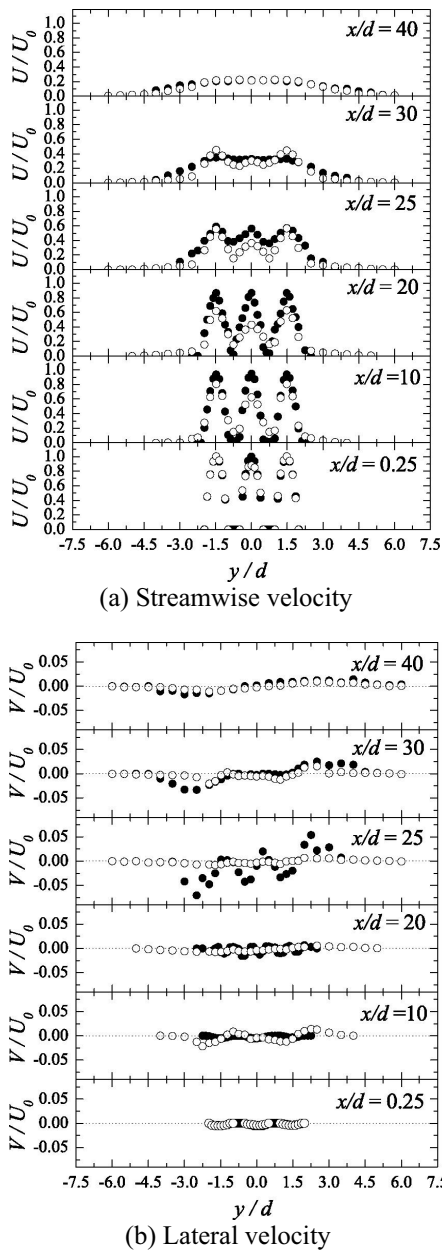
Fig. 7 Time-averaged velocity distributions of triple jet (o: perturbed jet, •: steady jet, Re = 1,500).

An unexpected but interesting feature characterizing the present jet perturbation was observed at the location, $x/d = 30$, where an adverse situation of the jet mixing trend between the steady and perturbed jet cases appears. That is, the steady jet case has a relatively flatter and wider velocity distribution without a cusp shape than the perturbed jet case. This implies that the steady jet diffuses more and the perturbed jet apparently suppresses the fluid mixing at this location. Point-symmetric distributions of the lateral

velocity were distinguishably observed there and also at x/d = 25 in the steady jet case of Fig. 7 (b), confirming again that the considerable spanwise diffusion occurs in the steady jet case.

In order to elucidate the above-mentioned adverse mixing situation, phase-averaged velocities of the perturbed jet case were calculated using the same time-sequential raw velocity data as the one for the calculation of time-averaged velocity plotted with o in Fig. 7 (a). After calculating the phase-averaged velocities at each measuring location, the time-averaged velocity was calculated for each aforementioned-categorized time-period, F-, O-, B- or C-region. Two graphs, (a) and (b), plotted with ◊ in Fig. 8 show the spanwise distributions of such phase-averaged and categorized streamwise velocity for O-region and C-region, respectively. The solid circle, •, denotes the steady jet case as the reference data for the comparison to the perturbed jet case. O-region corresponds to the time-period including the occurrence of maximum mass flow rate of C-jet, while C-region corresponds to the time-period of the minimum rate. F- and B-regions were found to have relatively similar velocity profiles to the steady jet case. Typical flow patterns of O-region were visualized as the snapshots #3 and #8 shown in Fig. 5, and the ones of C-region as the snapshots #1 and #6 (or #5 and #10).

A protruding velocity profile of C-jet in the case of the jet perturbation was seen at $x/d = 0.25$ in Fig. 8 (a), since the mass flow rate becomes relatively larger during O-region than the other regions, F, B and C. Hence, the jet Reynolds number becomes larger and the C-jet makes the transition from laminar to turbulent flow near the nozzle exit. Correspondingly, the mixing of the triple jet is enhanced and the jet fluid merges into one already at x/d = 20, so that the velocity distributions at further downstream locations have a hill-like shape with a gentle and wide slope, which appears better for the mixing than the velocity distribution of the steady jet case.

Focusing on the velocity distributions during C-region shown in Fig. 8 (b), on the other hand, their distribution patterns appear oppositely different from the ones during O-region. The mass flow rate of C-jet is relatively smaller during C-region, and the corresponding jet Reynolds number is in the regime of laminar flow. Hence, the C-jet remains laminar even at the location of x/d = 30. S-jets also remain laminar with almost no interaction with the comparatively lower velocity of C-jet, which leads to the velocity distribution possessing two high side-peaks and a relatively lower central peak, clearly seen at x/d = 25 and 30.

In contrast, the steady case of all the three jets possessing the same mass flow rate exhibits a three-peak-mountain-like velocity distribution of the triple jet flow somewhat interacting and merging together at x/d = 25. Then, at x/d = 30, an almost complete merging with C-jet and S-jets can be clearly seen in the result plotted with •, showing that the velocity distribution of this case forms a flatter and wider hill-like pattern.

In the case where the time-averaged velocity without the consideration of the phase is discussed, the effect of the C-jet during O-region is relatively conspicuous in the near-field of the jet nozzle exit because of turbulent jet, and a

better mixing among the triple jet is attained in comparison to the steady jet case. In further downstream of the nozzle exit, in contrary, no interaction among the individual laminar C-jet and S-jets during C-region leads to the suppression of the jet fluid mixing. Thus, the perturbed jet case apparently exhibits a smaller diffusion than the steady jet case. The r.m.s values of the velocity fluctuations were also correspondingly reversed between the steady and perturbed jet cases, figures of which were omitted because of the limited space. This interesting adverse characteristic of the jet perturbation can be applicable in respect of fluid mixing control.

CONCLUSIONS

Effects of a jet perturbation on the mixing performance of triple air-jet array have been experimentally investigated under the flow conditions of $Re = 1,500$ and $f_r = 0$, 1 or 2Hz in the present study. The major findings are summarized as follows:

1) The triple jet array discharged simultaneously in the steady case exhibits better mixing than the linearly-predicted jet array with three arithmetically-superimposed single jets.

2) The time-averaged velocity profiles of the triple jet array obtained in the present flow condition of jet perturbation demonstrate that a better mixing occurs in the near-field of the jet nozzle exit while the steady jet case has a better mixing performance in the further downstream, $x/d \geq 30$.

3) The adverse change of the mixing performance along the streamwise locations mentioned in the above item is related to the phase-averaged velocity profiles of the jet perturbation. Alternative change between laminar flow with smaller jet velocity and turbulent flow with higher jet velocity in one cycle of the central jet perturbation significantly influences and controls the time-averaged jet mixing performance.

NOMENCLATURE

A	perturbation amplitude, m/s
d	nozzle diameter, m
fr	perturbation frequency, Hz
L	separation distance between nozzles, m
Re	jet Reynolds number, $U_m d/v$
S	cross-sectional area of nozzle, m^2
U	time-averaged streamwise velocity of jet, m/s
U', u'	streamwise velocity fluctuation, m/s
V	time-averaged lateral velocity of jet, m/s
V', v'	lateral velocity fluctuation, m/s
x	streamwise distance, m
y	lateral distance, normal to jet axis, m

Greek symbols

v	kinetic viscosity of the fluid, m^2/s

Subscripts

m	time-averaged value
0	time-averaged reference value at the jet center

Superscripts

~	phase-averaged value

ACKNOWLEDGEMENT

REFERENCES

[1] Shinohara, E., Tatsumi, K., Okamoto, F., Kitaoka Y. and Nakabe, K., Mixing Characteristics of multi-jets modified by cyclic perturbation, *Proc. Int'l Conf. on Jets, Wakes and Separated Flows*, (2005), pp. 255 – 260.
[2] Durst, F., Ünsal, B. et al., Mass flow rate control system for tim-dependent laminar and turbulent flow investigations, *Measurement Sci. Technol.*, 14 (2003), pp. 893 – 902: Mass flow rate controlled fully developed laminar pulsating pipe flows, *ASME: J. Fluid Engineering*, 127 (2005), pp. 405 – 418: Pulsating laminar pipe flows with sinusoidal mass flux variations, *Fluid Dynamics Research*, 37-5 (2005), pp. 317 – 333.
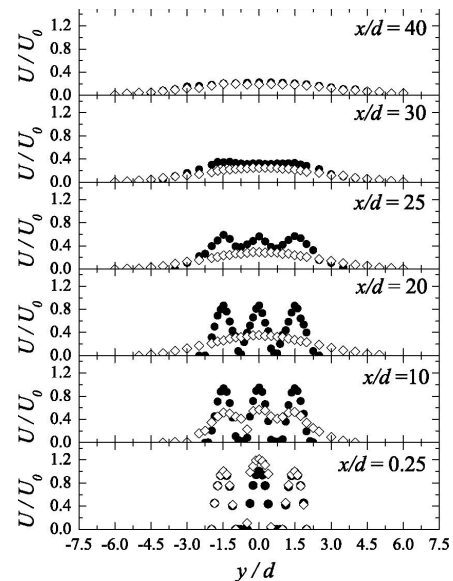
(a) Streamwise velocity of O-region
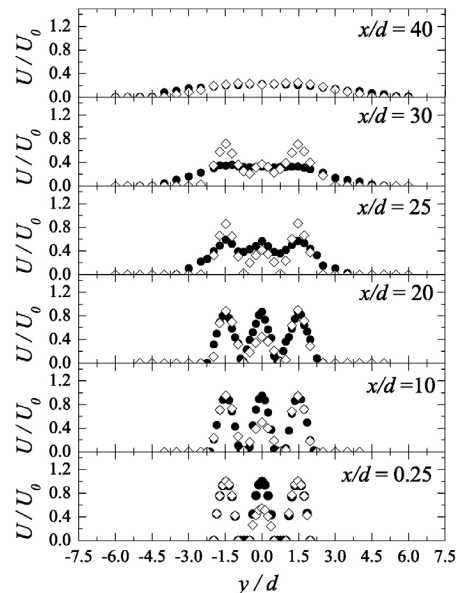
(b) Streamwise velocity of C-region

Fig. 8 Phase-averaged and categorized velocity distributions of triple jet ($\diamond$: perturbed jet, $\bullet$: steady jet, $Re = 1,500$).